JACS
JOURNAL OF THE AMERICAN CHEMICAL SOCIETY
Article
pubs.acs.org/JACS

Oriented Gold Nanoparticle Aggregation for Colorimetric Sensors with Surprisingly High Analytical Figures of Merit

Longhua Guo,[†] Yang Xu,[†] Abdul Rahim Ferhan,[‡] Guonan Chen,*[,†] and Dong-Hwan Kim*[,‡]

[†]Ministry of Education Key Laboratory of Analysis and Detection Technology for Food Safety, Department of Chemistry, Fuzhou University, Fuzhou, 350108, China

[‡]School of Chemical and Biomedical Engineering, Nanyang Technological University, 637457, Singapore

ABSTRACT: The common drawbacks of current colorimetric sensors using gold nanoparticle aggregation is its relatively low sensitivity and narrow dynamic range, which restrict their application in real sample analysis when competing with other analytical techniques such as fluorescence and chemiluminescence. In this article, we demonstrate a novel strategy to construct colorimetric sensors based on gold nanoparticle aggregation. Unlike the conventional colorimetric sensors which cause the formation of large nanoparticle aggregates, in our strategy, dimers are selectively formed upon target binding, which results in significantly improved long-term stability and a more than 2 orders of magnitude wider dynamic range of detection than that of the conventional colorimetric sensors. In addition, a strategy to minimize the interparticle gap through the formation of a Y-shaped DNA duplex enables to increase the limit of detection by 10 000 times. The analytical figures of merit of the proposed sensor are comparable to those of the fluorescence-based sensors.

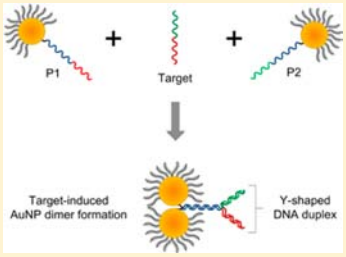

1. INTRODUCTION

Spherical gold nanoparticles (AuNPs) in solution appear red due to their intense surface-plasmon resonance at ~520 nm. The aggregation of AuNPs induces an electric dipole−dipole interaction and coupling between the plasmons of neighboring particles, causing the color to change to purple or blue.[1,2] Based on this principle, numerous colorimetric sensors that utilize a measurable color change as a quantification tool have been developed.[3,4] The target molecules vary from biomolecules (proteins[5−9] and nucleic acids[10,11]) to small organic molecules[12,13] and metal ions.[14−16] The advantages of colorimetric sensors include the following: (i) They are easy to use; homogeneous colorimetric detection typically involves a single step without requiring trained personnel. (ii) They are cost-effective; only a few nanoparticles are needed to generate visible color changes due to the extremely high extinction coefficients (typically 4 orders of magnitude larger than those of organic dyes[17]). (iii) Neither complex nor expensive analytical instruments are needed; a portable UV−vis spectrometer can be used for localized surface plasmon resonance (LSPR) extinction detection, and the target concentration can be qualitatively estimated from the color change using the naked eye.

Despite the many advantages, long-standing challenges associated with nanoparticle aggregation-based colorimetric sensors remain, which restrict their application in real sample analysis. First, the aggregation of cross-linked nanoparticles is nondirective, resulting in the formation of large, long-range aggregates.[18] A suspension of these aggregates is unstable in solution due to the increased particle size and reduced surface repelling force. Thus, the color of the suspension diminishes over time, becoming colorless in a few hours due to the settlement of the nanoparticle aggregates.[19] This time-dependent color change prevents accurate target determination because the duration of the experiment must be fixed when performing the assays to obtain comparable data across various samples. Another limitation of a large-aggregate sensor is its relatively low sensitivity. Previous theoretical investigations and experimental data have indicated that a molar excess of the target molecule over the nanoparticles is necessary to achieve a detectable colorimetric shift.[18,20,21] Although detection sensitivity can be improved by the use of relatively big nanoparticles,[22,23] the long-term stability of sensors tends to be inversely proportional to nanoparticle size; hence, small nanoparticles (e.g., 10−20 nm in diameter) have been commonly used to achieve a compromise between sensitivity and stability. Consecutively, most of the reported approaches based on AuNP aggregation have a limit of detection (LOD) worse than 5 nM. This LOD is several orders of magnitude poorer than that of the widely used fluorescent-based sensors.[24] Additionally, the typical dynamic range of detection for nanoparticle aggregation-based sensors is only 1 to 2 orders of magnitude, which is also much narrower than that of fluorescence-based approaches.[25−27]

To address these issues, a variety of approaches have been introduced. For example, AuNP-based detection strategies have been coupled with the reduction of silver(I) to provide signal amplification leading to a LOD improvement by several orders of magnitude.[28,29] In addition, Ginger and co-workers demonstrated optical sensing of DNAs[30] and proteins[31] in complex media via DNA-functionalized AuNP dimers immo-

Received: May 29, 2013
Published: July 26, 2013

   dx.doi.org/10.1021/ja405371g | J. Am. Chem. Soc. 2013, 135, 12338−12345

bilized on a substrate. Storhoff and co-workers showed that the colorimetric response can effectively be enhanced when target-induced AuNP aggregation is performed on a white support[32] or an illuminated glass waveguide,[20] of which it provided a lasting record for each test. Recently, Lim and co-workers[33] reported a signal amplification strategy to enhance visible detection by controlling the extent of nanoparticle aggregation.

In this contribution, we propose a novel approach for constructing a colorimetric sensor that renders a tailored interparticle distance and a controlled aggregate size. We present (1) a method to orient the nanoparticle aggregates, as asymmetrically PEGylated AuNPs are utilized to selectively form dimers without forming large aggregates upon target binding, which results in significantly improved long-term stability and a wider dynamic range of detection, and (2) a strategy to minimize the interparticle gap through the formation of a Y-shaped DNA duplex, which improves the limit of detection by orders of magnitude.

2. EXPERIMENTAL SECTION

2.1. Chemicals and Solutions. All oligonucleotides were synthesized by Sangon Biotech Co., Ltd. (Shanghai). The genomic DNA isolated from *Vibrio cholerae* and *Escherichia coli* bacterial cells was purchased from ATCC. Tris[2-carboxyethyl]phosphine (TCEP), sodium dodecyl sulfate (SDS), and tris(hydroxymethyl)aminomethane hydrochloride (Tris) were supplied by Merck Pte., Ltd. Sodium citrate, poly(ethylene glycol) 2-thioethyl ether acetic acid (thiol-PEG-acid, average M_n 1000), gold(III) chloride trihydrate (99.9%), formamide, dextran sulfate, and ascorbic acid were purchased from Sigma-Aldrich Pte., Ltd. Other chemicals were purchased from Sinopharm Chemical Reagent Co., Ltd. The hybridization buffer was a 20 mM Tris buffer solution (pH 7.4) containing 15% formamide, 10% dextran sulfate, 0.3 M NaCl, and 3.75 mM $MgCl_2$. Probe and target sequences used in this work are shown in Scheme 1.

2.2. Procedures for Asymmetrical Modification of AuNPs. AuNPs with an average diameter of 43 nm were synthesized via the sodium citrate reduction of $HAuCl_4$ as previously described.[34] Procedures for fabricating the asymmetrically functionalized AuNPs were divided into the following five steps: (1) A glass coverslip was first activated by immersing it in a "piranha" solution (30% H_2O_2 mixed in a 1:4 ratio with concentrated H_2SO_4) for 15 min. The coverslip was then washed thoroughly with distilled water and stored in ethanol prior to use. (2) The activated coverslip was immersed in a solution containing 0.05 M CTAB for 30 min and then washed three times with distilled water. (3) The CTAB-modified glass coverslip was then immersed in the citrate-stabilized 43-nm AuNP (which is negatively charged) solution for 5 min. The glass substrate was then removed and washed with water three times to remove any loosely bound AuNPs. (4) The AuNP-modified glass substrate was then immersed in a 10 mM thiol-PEG-acid solution (0.1 M phosphate buffer, pH 8.0) and incubated for 24 h. The substrate was then removed and washed thoroughly with water to remove any loosely bound PEG. (5) To remove the particles from the glass substrate after modification, the substrate was sonicated in 1.0 mL water for 1 min, resulting in a dispersion containing PEG asymmetrically functionalized AuNPs.

Scheme 1. Oligonucleotides Used in This Work

a. Oligonucleotides used for the oriented sensor

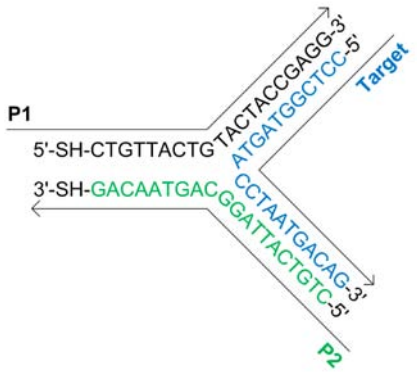

1-bp mismatch: 5'-CCT CGG TAG TAT CTA ATG ACA G-3'
2-bp mismatch: 5'-CCT CGG TAG TGT CTA ATG ACA G-3'
Total mismatch: 5'-GAC TCA GGC ATG GAC CGT TCC A-3'

b. Oligonucleotides used for the non-oriented sensor

P1' 3'-SH-$(T)_6$-GGA GCC ATC AT-5'
Target 5'-CCT CGG TAG TAC CTA ATG ACA G-3'
P2' 3'-G GAT TAC TGT C-$(T)_6$-SH-5'

2.3. AuNP Characterization. The scanning electron microscopy (SEM) images were obtained using an FE-SEM (Nova NanoSEM 230, FEI Co., Hillsboro, OR) at an acceleration voltage of 10.0 kV and a working distance of 6−8 mm. The samples were physically immobilized on silicon wafers and were observed under FE-SEM without platinum coating. To prepare the AuNP dimer samples for SEM, the sample solution was diluted 20-fold to obtain monodispersed AuNP dimers.

2.4. Spectral Measurements. A portable UV−vis spectrophotometer (Maya2000 Pro) purchased from Ocean Optics (Dunedin, FL) was used for all absorbance measurements. A tungsten halogen light source (LS-1) was used to generate the LSPR, and two optical fiber bundles (P400−2-VIS-NIR) were used for optical transmission. An optical flow cell with a "Z" configuration (FIA-Z-SMA-SS, 10-mm path length with a volume of 50 μL) was used for sample loading. The LSPR measurements were performed in a transmission mode using the UV−vis spectrophotometer at wavelengths ranging from 400 to 900 nm at room temperature. The melting experiments were carried out at 0.5 °C intervals.

2.5. Probe Immobilization. Prior to modification of the oligonucleotide, the thiol groups were activated according to a method described in literature.[35] The 5′-thiol oligonucleotides (0.1 mM) were deprotected with 0.l mM tris(2-carboxyethyl)phosphine (TCEP) in 20 mM Tris buffer (pH 7.4) for 1 h at room temperature. A 100 μL aliquot of the deprotected oligonucleotides (100 μM) was then mixed with a 1-mL PEG asymmetrically functionalized AuNP solution (20 mM Tris (pH 7.4), 100 pM AuNP, 0.01% SDS). The oligonucleotide/gold nanoparticle solution was incubated overnight at room temperature. Aqueous NaCl (2.0 M with 0.01% SDS) was then added to the solution to bring its total NaCl concentration to 0.1 M. The mixture was again incubated for 5 h. The NaCl concentration was increased to 0.2 M using the same approach and incubated for another 5 h. Then the NaCl concentration was raised to 0.3 M. After additional 5-h incubation, the gold nanoparticle solution was centrifuged and the supernatant removed leaving a pellet of gold nanoparticles at the bottom. The particles were then resuspended in 1 mL of hybridization buffer. This washing process was repeated three times.

2.6. Target Detection with AuNP Probes. The target sequence detection was carried out as follows: 30 μL of the target oligonucleotide at the stated concentration was combined with 30 μL of the hybridization buffer and 40 μL of AuNP probes (AuNPs modified with P1 and P2 were mixed at a 1:1 ratio with a final AuNP concentration of 30 pM). The solution was heated to 68 °C for 60 s and incubated at the operating temperature (37 °C for single-bp mismatch discrimination and 25 °C for the others). The absorbances of 50-μL aliquots of the target and control samples were measured using an FIA-Z-SMA-SS optical flow cell (50-μL volume, 10-mm path length).

For pathogenic DNA detection, the genomic DNA isolated from *Vibrio cholerae* was resuspended in 20 mM Tris buffer (pH 7.4) with a

dx.doi.org/10.1021/ja405371g | J. Am. Chem. Soc. 2013, 135, 12338−12345

final concentration of 0.1 $\mu g/\mu L$. The solution was then sonicated at 4 °C using 20 consecutive 30-s-on, 30-s-off cycles at low power (UCD200-Bioruptor) to fragment the long chains. The fragmented DNA was diluted with Tris buffer (20 mM, pH 7.4) to the stated final concentration. The genomic DNA isolated from *Escherichia coli* was utilized as the negative control to estimate the specificity of the sensor.

2.7. Calculation of LOD. To obtain our LOD, we use an IUPAC-recommended methodology that utilizes an experimentally determined signal-to-noise ratio (S/N).[36,37] The absorbance at designated wavelengths (i.e., 600 nm for the oriented sensor and 620 nm for the nonoriented sensor) of a control sample containing AuNP probes without target oligonucleotides was measured 20 times. Based on this, an average absorbance for blank ($\text{average}_{\text{blank}}$) along with the associated standard deviation (SD_{blank}) was determined. This SD_{blank} was regarded as the noise (N) of our detection system. Next, detection was performed from samples with a known, relatively low concentration of target sequences. The resultant absorbance at the same wavelength (i.e., 600 or 620 nm) was measured five times, and the average value ($\text{average}_{\text{sample}}$) was calculated. Finally, S/N was calculated as follows:

$$\text{S/N} = (\text{average}_{\text{sample}} - \text{average}_{\text{blank}})/\text{SD}_{\text{blank}}$$

If the S/N was greater than 5, the sample was diluted to half the initial concentration and the S/N determination was repeated until the S/N value fell within the range of 3 to 5. A sample concentration that meets the condition of $3 < \text{S/N} < 5$ was determined as the LOD of our detection platform.

3. RESULTS AND DISCUSSION

3.1. Principle of Sensor. The fabrication of the proposed sensor can be divided into two major steps: asymmetrical modification of the AuNPs with PEG and probe attachment. The asymmetrical modification is depicted in Scheme 2a. Citrate-stabilized 43-nm AuNPs were immobilized onto a glass substrate modified with a hexadecyl trimethylammonium bromide (CTAB) bilayer through an electrostatic attraction. The substrate was then immersed in a solution containing PEG-thiols. A dense PEG monolayer was formed on the surface of the AuNPs except those areas that were in contact with the substrate. After sonication in distilled water, a suspension of asymmetrically PEGylated AuNPs was obtained. The PEGylated AuNPs were used to construct AuNP dimers and as a proof-of-concept for detecting specific gene sequences in the foodborne pathogen, *Vibrio cholerae*. The detection mechanism is depicted in Scheme 1b. Two probes (designated as P1 and P2) were separately introduced onto the PEGylated AuNPs in two different solutions. The sequences of each probe contain two segments: one that is complementary to a portion of the sequences for the other probe, and another that is complementary to the target. When the P1-modified AuNPs and the P2-modified AuNPs are mixed, no DNA duplexes are constructed due to the small number of complementary segments in P1 and P2 because the melting temperature (T_m) is below the operating temperature (i.e., 25 °C), which prevents the formation of AuNP aggregates. However, in the presence of the target, perfect complementary Y-shaped DNA is formed because the T_m is above the operation temperature. During the formation of the Y-shaped DNA, the dispersed AuNPs aggregate into dimers due to the asymmetrical modification of the AuNPs, which is often observed with asymmetrically modified nanoparticles.[38−41]

Figure 1a demonstrates the changes in the extinction spectra of the AuNPs during the sensor fabrication. Prior to the asymmetrical modification, the citrate-protected 43-nm AuNPs exhibit a plasmon resonance peak at 528 nm (the black trace).

Scheme 2. Principle and Fabrication Procedures of the AuNP-Based Nucleic Acid Sensor Described in This Work (size not to scale)

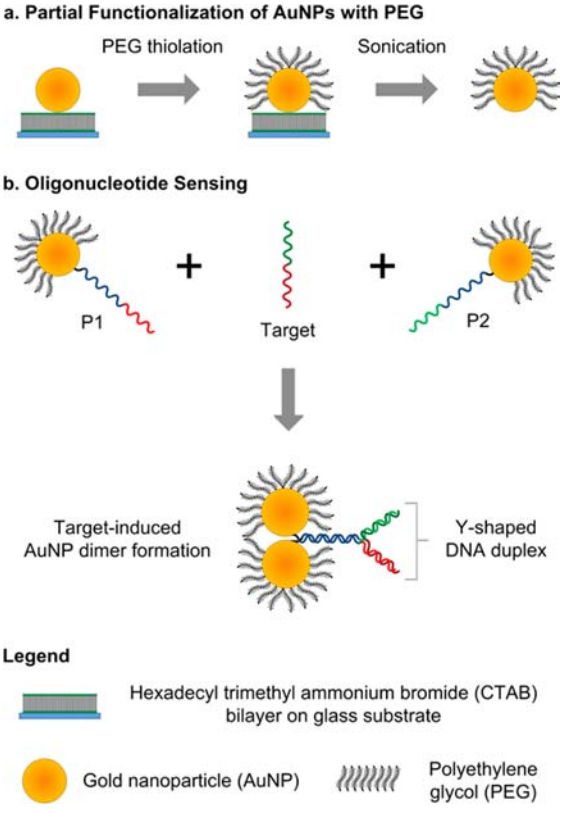

Replacing the citrate with PEG produces a dense organic layer on the AuNP surface, which significantly increases the localized refractive index.[42−45] Thus, the extinction of the AuNP plasmon resonance is red-shifted to 537 nm (the red trace). After introduction of a thiol-modified oligonucleotide (P1) onto the asymmetrically PEGylated AuNP surface, another 1.5-nm peak shift is observed, which is much smaller than the PEGylation-induced shift (9 nm). This slight peak shift is attributed to the fact that most of the AuNP surface has been occupied by PEG during the asymmetrical modification; hence, only a limited number of P1 is available to bind to a small region of the unmodified AuNP surface.

The total peak shift (or color change) generated by the binding of the target determines the sensitivity of the colorimetric sensors. The optical properties of the macroscopic AuNP aggregate are known to depend not only on the interparticle distance but also on the aggregate size.[18] Consequently, measurable shifts in the plasmon resonance can be observed even with the relatively long interparticle distances when a large aggregate is formed. In our sensor design, the formation of multimers and large aggregates is restrained due to the asymmetrical modification and the fact that a large majority of AuNPs form dimers upon target binding; thus, this dimer sensor is designated as an oriented sensor. The plasmon resonance peak shifts caused by the dimer formation are strictly related to the interparticle gap. For dimers formed by spherical nanoparticles, a smaller gap generally produces a larger peak shift.[46−49] Thus, reducing the interparticle distance to its smallest possible value is vital for obtaining visibly distinctive color changes. Previously, we reported a solid-phase, single-dimer-based nucleic acid switch

dx.doi.org/10.1021/ja405371g | J. Am. Chem. Soc. 2013, 135, 12338−12345

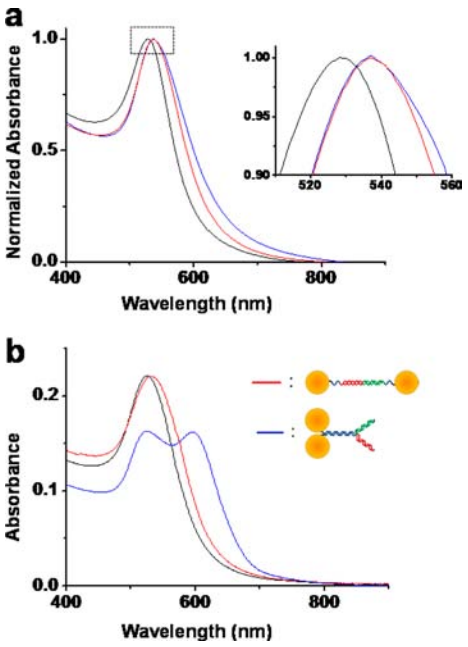

Figure 1. (a) Normalized optical absorption spectra for the AuNPs before (black trace) and after (red trace) immobilization of the PEG ligand and after immobilization of the DNA probes (P1, blue trace). The inset shows the enlarged portion of the area bounded by the dashed box. (b) Optical absorption spectra of the proposed sensor using a Y-shaped DNA linker (blue trace) and a sensor fabricated using the conventional strategy (red trace) upon binding to the targets (10 nM). The dimer linked with a Y-shaped DNA contains 15 pM P1-modified AuNPs and 15 pM P2-modified AuNPs; the sensor fabricated using the conventional strategy contains 15 pM P1′-modified AuNPs and 15 pM P2′-modified AuNPs.

that greatly improved the LSPR peak shift.[50] In this article, a strategy involving the formation of Y-shaped DNA is utilized to modulate the interparticle distance of the dimers for a colorimetric sensor in a homogeneous solution phase. As shown in Scheme 2b, after the addition of target DNA, three oligonucleotides (i.e., the target DNA, P1 and P2) form a Y-shaped DNA duplex. This DNA binding should drive the two linked AuNPs to approach each other. To verify that the Y-shaped DNA pulls the two nanoparticles closer than that for a linear DNA linker, we investigated the LSPR responses of the dimers fabricated with both the Y-shaped DNA and linear DNA (Figure 1b). An identical batch of asymmetrically modified AuNPs was used to minimize the size- and shape-dependent plasmonic variations between each experimental set. For the Y-shaped DNA, after adding the target sequences to the mixture containing the P1-modified AuNP (AuNP-P1) and P2-modified AuNP (AuNP-P2), an absorbance at ∼600 nm was observed (the blue trace in Figure 1b) in addition to the peak at 540 nm. The appearance of a second peak at ∼600 nm indicates a strong interparticle plasmon coupling between two adjacent AuNPs. The average interparticle distance of the coupled AuNPs was estimated to be less than 1 nm, as determined using a previously reported theoretical simulation.[48] It is also consistent with our previous report, in which a loop-structured DNA was used to construct dimers.[50] However, the addition of the same target concentration into a solution of P1′-modified AuNPs and P2′-modified AuNPs generated a slight peak shift due to a weak interparticle coupling effect (the red trace in Figure 1b). This result proves that the Y-shaped DNA duplex minimizes the interparticle distance between the linked AuNPs, resulting in a substantial plasmonic peak shift.

3.2. Analytical Figures of Merit. Next, we investigated the concentration-dependent response of the oriented sensor based on the Y-shaped DNA linked dimer. Aliquots of standard solutions containing concentrations of the target DNA ranging from 1 pM to 10 nM were tested, and the extinction spectra are presented in Figure 2a. As the target DNA concentration

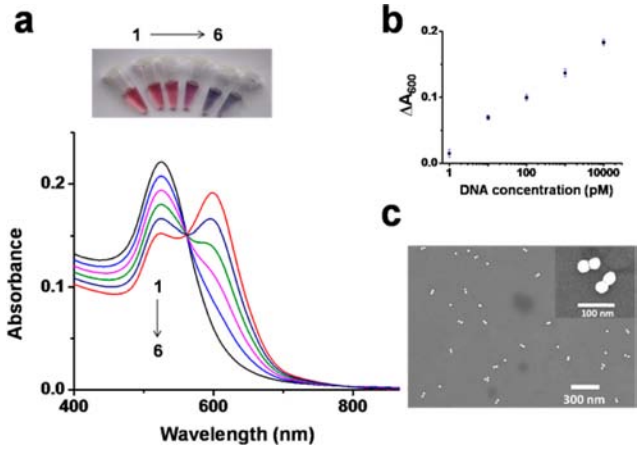

Figure 2. (a) Photographs and optical absorption spectra of the asymmetrically functionalized AuNPs (a solution containing 15 pM AuNP-P1 and 15 pM AuNP-P2) recorded 60 min after the addition of various concentrations of the target DNA (the target concentrations for the spectra from 1 to 6 are 0, 1 pM, 10 pM, 100 pM, 1 nM, and 10 nM, respectively). (b) A calibration curve corresponding to part a. The error bars represent the standard deviations for three replicates. (c) A representative SEM image of a sample containing 10 nM target DNA. The sample was prepared on a silicon wafer using a drop-and-dry method and tested without a platinum coating. Prior to dropping the sample onto the silicon wafer, the sample solution was diluted 20-fold to avoid spatial interference between individual AuNP dimers.

increased, the peak at 600 nm, a peak characteristic of dimers, increased, while the extinction at 540 nm, a peak characteristic of Au nanospheres, decreased. To directly compare these results to those of conventional colorimetric sensors based on random AuNP aggregation,[4,5,10,11,51−58] we also fabricated a sensor using a previously reported approach with the same batch of 43-nm AuNPs (designated as a nonoriented sensor).[59,60] Unlike the asymmetric modification in our sensor, this conventional, nonoriented sensor utilized the AuNPs, the full surface of which is symmetrically modified with the probe molecules. The results of a titration experiment with the nonoriented sensor are provided in Figure 3a. As expected, the nonoriented sensor induces large aggregates upon binding with the target (Figure 3c), causing a broad extinction peak beyond 620 nm with no second peak at 600 nm regardless of the target concentration. This result differs dramatically from the twin-peak development generated by our oriented sensor, in which a sharp peak appears at ∼600 nm and its absorbance intensity increases with increasing target concentration. This difference in the obtained spectra indicates that different LSPR coupling events occur between the nonoriented and oriented sensors. As shown in Figure 2c, neither a nonspherical Au nanoparticle nor a multimer is observed; hence, the second peak at ∼600 nm evidently originates from the coupling of spectra of the AuNP dimers. We note that most colorimetric sensors based on nanoparticle aggregation exhibit LODs above 5 nM.[10−12,61−68]

dx.doi.org/10.1021/ja405371g | J. Am. Chem. Soc. 2013, 135, 12338−12345

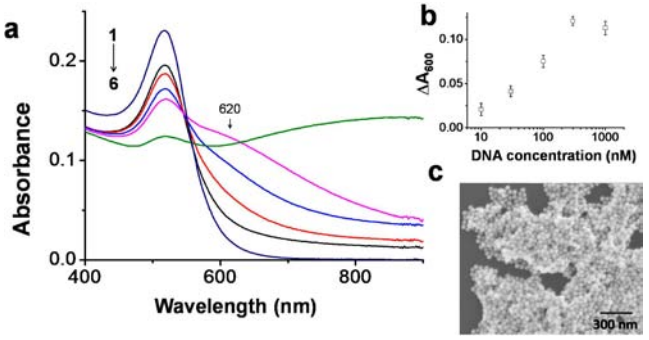

Figure 3. (a) Optical absorption spectra of the nonoriented sensor fabricated using a previously reported approach[59] recorded 60 min after the addition of various concentrations of the target DNA (the concentrations of spectra 1 to 6 are 0, 10 nM, 30 nM, 100 nM, 300 nM, and 1000 nM, respectively). (b) Calibration curve corresponding to part a. The error bars represent the standard deviations of three replicates. (c) A typical SEM image of a sample containing 300 nM target DNA. The sample was prepared on a silicon wafer using a drop-and-dry method and tested without a platinum coating.

For the purpose of verification, the LOD we obtained for nonoriented sensor was 10 nM (S/N = 3.3), which was 10 000 times worse than that of our oriented sensor (1.0 pM (S/N = 4.6), as shown in Figure 2b). This extraordinary improvement in sensitivity can be explained as follows: For a nonoriented sensor, the interparticle distance is not small enough to generate detectable peak shifts when small aggregates are formed. Therefore, a colorimetric change can be observed only when a molar excess of the target is available. Thus, targets at a low concentration cannot be detected. In the oriented sensor, even low target-molecule concentrations can induce dimer formation. Due to the small interparticle distance generated by the Y-shaped DNA structure, a significant peak shift occurs when dimers are formed; thus, a target can be detected even at extremely low concentrations.

Furthermore, a surprisingly large dynamic range from 1.0 pM to 10 nM was observed in the oriented sensor. In comparison, the nonoriented sensor exhibited a dynamic range from 10 nM to 300 nM under the same experimental conditions used for the oriented sensor and in previous literature.[10−12,61−66,68] When the target concentration is above 300 nM, the absorbance of the nonoriented sensor at 620 nm (A_{620}) no longer increases, but a slight decrease in A_{620} is observed (the green line in Figure 3a). This result suggests that, when the target concentration is above 300 nM, any further increase in target concentration do not cause new aggregates to form through the short-range interaction. Instead, the increase induces the relatively small, preformed aggregates to cluster into larger aggregates. The large aggregates have a maximum absorbance peak in the near-infrared region, decreasing the A_{620}.

The improved dynamic range of the oriented sensor over that of the nonoriented sensor (more than 2 orders of magnitude) can be attributed to the following: (1) Unlike the oriented sensor, the nonoriented sensor cannot detect low target concentrations. (2) The dispersed AuNPs in the nonoriented sensor form large aggregates with high target concentrations and thus precipitate whereas the AuNP-dimers formed in the oriented sensor do not precipitate. No such highly improved figure of merit (e.g., LOD and dynamic range) has been achieved for a nanoparticle-aggregation-based sensor. In addition, the analytical figures of merit of the oriented sensor are comparable to those of the fluorescent DNA sensors that employ complex and expensive enzyme-based targets or signal-amplification.[69−72] In comparison, our approach is simple, is inexpensive, and can achieve qualitative assays with the naked eye due to the significant color changes upon target binding. Therefore, the oriented sensor proposed in the present study can potentially be applied to clinical nucleic acid diagnostics which is currently dominated by fluorescence-based methods.

To evaluate the long-term, postdetection stability, we compared the time-dependent LSPR response of the oriented- and the nonoriented sensors (Figure 4). For a comparison at

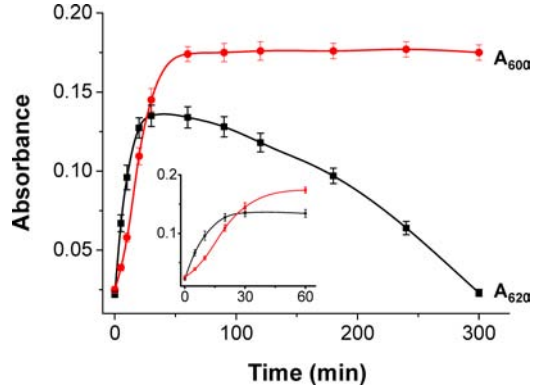

Figure 4. Change in absorbance of the oriented sensor (15 pM AuNP-P1 and 15 pM AuNP-P2, red curve) and the nonoriented sensor (15 pM AuNP-P1 and 15 pM AuNP-P2, black curve) with respect to time after the addition of the target DNA (10 nM for the oriented sensor and 300 nM for the nonoriented sensor in the final solution). The oriented sensor was monitored at 600 nm, while the nonoriented sensor was monitored at 620 nm to obtain the maximum change in absorbance. The scale bars represent the standard deviations of three replicates.

the maximum absorbance, the oriented sensor and the nonoriented sensor were monitored at 600 nm (A_{600}) and 620 nm (A_{620}), respectively. After the target molecule (10 nM for the oriented sensor and 1 μM for the nonoriented sensor, the highest concentrations tested) was added, the absorbance increased rapidly for both sensors at their respective wavelengths. The slope of the nonoriented sensor was steeper than that of the oriented sensor within the first 20 min, which indicated that the reaction speed of the nonoriented sensor is greater than that of the oriented sensor in the initial stage. The A_{600} of the oriented sensor reached a stable plateau after 60 min, indicating that a dynamic equilibrium had been achieved. The A_{620} of the nonoriented sensor, however, began to decrease 60 min after reaching equilibrium, which could be attributed to the following: (1) small aggregates grow into large aggregates during this period, which induces a further red shift of the extinction spectra, and (2) the precipitation of large aggregates results in a decrease in the absorbance. The nonoriented sensor became colorless after 5 h, indicating that most of the AuNPs in the solution have precipitated. In comparison, the A_{600} of the oriented sensor remained stable for 48 h after the addition of the targets. These results prove that the design of the oriented dimer using asymmetrical PEG modification of the AuNPs guides the nanoparticle aggregation in a controlled manner and improves the stability of the sensor, which, in turn, helps to reduce the variation in sensitivity across different assays.

The environmental stability of a biosensor in a complex matrix, e.g., in the presence of high-molecular-weight DNA

dx.doi.org/10.1021/ja405371g | J. Am. Chem. Soc. 2013, 135, 12338−12345

and/or in solutions that span a wide range of electrolyte concentration, is vital for biomedical applications. We, therefore, investigated the analytical performance of the proposed sensor in solutions containing various concentrations of NaCl and calf thymus DNA. The oriented sensor was stable in solutions with high salt concentrations of up to 2.0 M NaCl (Figure 5a). Similarly, the LSPR responses of the oriented

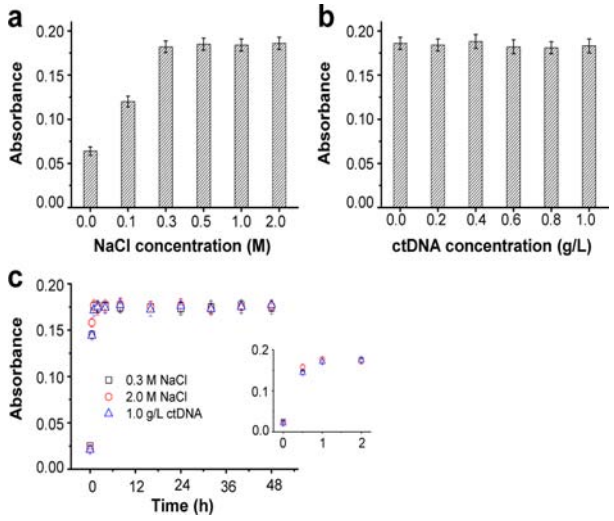

Figure 5. Environmental stability of the sensor (15 pM AuNP-P1, 15 pM AuNP-P2) in NaCl (a), ct-DNA (b), and the long-term stability of the sensor in NaCl and ct-DNA (c). The cDNA concentration was 10 nM for all experiments. The final NaCl concentration in all experiments in b was 0.3 M. The scale bars represent the standard deviations of three replicates.

sensor did not vary in solutions containing calf thymus DNA up to 1.0 g/L (Figure 5b). This stability could be attributed to the PEG modification on the AuNP surface. Replacing citrate with PEG can effectively enhance the dispersibility of the AuNPs in aqueous solutions as reported in the literature.[73−75] The long-term stability of the oriented sensor was also investigated in solutions containing varying quantities of NaCl and calf thymus DNA, and the results indicate that the A_{600} of all sensors remains nearly unchanged even after storage for 48 h (Figure 5c).

The target selectivity is another important sensor parameter. We investigated the selectivity of the oriented sensor for detecting DNA strands in perfect complementary (cDNA), 1-bp mismatch, 2-bp mismatch, and complete mismatch (Figure 6). At room temperature, the sensor can distinguish the target cDNA from DNA sequences containing an at least 2-bp mismatch. However, the LSPR response for the sample with a 1-bp mismatch was not selective (~75% of the signal from the cDNA). We found that the melting temperature of the solution containing the cDNA was 49.5 °C but was 27.2 °C with a 1-bp mismatch (Figure 6 inset). Therefore, taking advantage of the large disparity in the melting temperature, even DNA sequences with a single-bp mismatch can be conveniently screened by controlling the operating temperature.

3.3. Foodborne Pathogen Assay. Finally, to evaluate the feasibility of the oriented sensor for rapid and ultrasensitive nucleic acid assays, we demonstrated the detection of unamplified genomic DNA isolated from *Vibrio cholerae*. *Vibrio cholerae* bacteria are foodborne pathogens typically responsible for cholera, a common diarrheal illness. Cholera is the leading

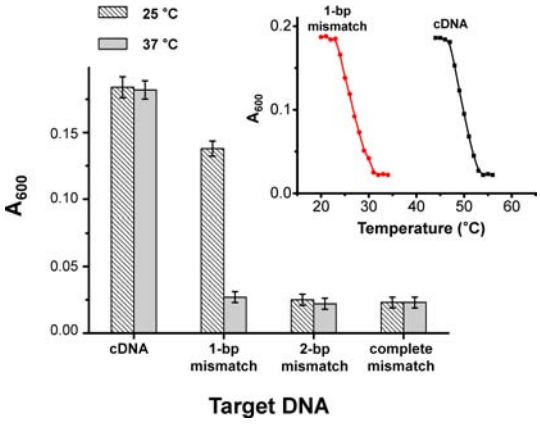

Figure 6. Selectivity study of the oriented sensor at different operating temperatures to analyze the cDNA and DNA sequences with 1-bp, 2-bp, and total mismatch. The inset shows the melting curves of the solutions containing cDNA and DNA sequences with 1-bp mismatch. The DNA sequences are as follows: cDNA: CCT CGG TAG TAC CTA ATG ACA G; 1-bp mismatch: CCT CGG TAG TAT CTA ATG ACA G; 2-bp mismatch: CCT CGG TAG TGT CTA ATG ACA G; total mismatch: GAC TCA GGC ATG GAC CGT TCC A. Each sensor contains 15 pM AuNP-P1, 15 pM AuNP-P2, and 10 nM target sequences in the final solution.

cause of morbidity and mortality in many developing countries.[76,77] Culture-based methods are predominantly used to characterize *Vibrio cholerae* in food and clinical samples. However, these methods are limited by the relatively long time required for analysis (usually 2−3 days).[78] We demonstrate a dimer-based colorimetric sensor for the direct detection of cholera-specific sequences. Prior to detection, the genomic DNA was fragmented using sonication. The fragmented DNA was diluted with a hybridization buffer to the stated final concentration and mixed with a solution containing P1- and P2-modified AuNPs in a 1:1 volume ratio. A detectable color change (A_{600}) was obtained in a solution containing 2 ng/μL *Vibrio cholerae* genomic DNA, while no observable color change was observed in the negative control containing 500 ng/μL total genomic DNA isolated from *Escherichia coli* (Figure 7). The results strongly indicate the oriented sensor possesses high selectivity in the presence of complex DNA. The ability for sensitive and selective analysis of unamplified genomic DNA demonstrates the potential of the proposed sensor for nucleic acid detection in a variety of applications such as environmental monitoring, food safety control, and clinical diagnostics.

4. CONCLUSIONS

In summary, our work demonstrated the use of an ultrasensitive biosensor for the homogeneous, quantitative, and colorimetric detection of nucleic acid sequences based on the target oligonucleotide-induced formation of AuNP dimers. The proposed sensor differs from previously reported AuNP-based colorimetric biosensors in several respects: (1) The addition of the target causes dimers to form due to the use of asymmetrical PEG-modified AuNPs. The strategy to restrain the multimer formation not only greatly enhances the long-term stability of the sensor but also improves the dynamic range of detection by more than 2 orders of magnitude. (2) The proposed sensor is 10 000 times more sensitive than a sensor fabricated using conventional strategies. This significant improvement in sensitivity can be largely attributed to the Y-shaped DNA duplex, the formation of which enables two linked AuNPs to be

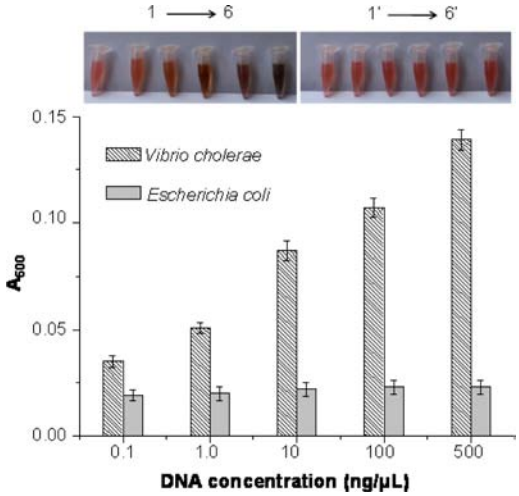

Figure 7. Selectivity of the sensors (15 pM AuNP-P1, 15 pM AuNP-P2) for testing concentrations of *Vibrio cholerae* and *Escherichia coli* genomic DNA that varies from 0.1 ng/μL to 500 ng/μL. The scale bars represent the standard deviations of three replicates. The photos on top show color changes of the oriented sensor corresponding to the binding of different concentration of *Vibrio cholerae* (1−6) and *Escherichia coli* (1′−6′) genomic DNA (the genomic DNA concentrations of 1−6 and 1′−6′ are 0, 0.1, 1.0, 10, 100, and 500 ng/μL, respectively).

pulled to a closest distance yielding the maximum color change. In addition, the ability of the sensor to rapidly detect unamplified genomic DNA isolated from foodborne pathogens in a complex sample matrix has successfully been demonstrated.

AUTHOR INFORMATION

Corresponding Author

gnchen@fzu.edu.cn; dhkim@ntu.edu.sg

Notes

The authors declare no competing financial interest.

ACKNOWLEDGMENTS

The authors gratefully acknowledge the financial support of the 973 Program of China (2010CB732403), National Natural Science Foundation of China (21205017, 21277025, 21275031, 21222506), Natural Science Foundation of Fujian Province (2012J01036), and the Foundation of Fujian Educational Committee (JA12039). D.H.K. acknowledges the financial support of the Ministry of Education of Singapore (MOE2012-T2-1-058)

REFERENCES

(1) Murphy, C. J.; Gole, A. M.; Stone, J. W.; Sisco, P. N.; Alkilany, A. M.; Goldsmith, E. C.; Baxter, S. C. *Acc. Chem. Res.* **2008**, *41*, 1721.
(2) Ghosh, S. K.; Pal, T. *Chem. Rev.* **2007**, *107*, 4797.
(3) Sperling, R. A.; Gil, P. R.; Zhang, F.; Zanella, M.; Parak, W. J. *Chem. Soc. Rev.* **2008**, *37*, 1896.
(4) Xia, F.; Zuo, X.; Yang, R.; Xiao, Y.; Kang, D.; Vallée-Bélisle, A.; Gong, X.; Yuen, J. D.; Hsu, B. B. Y.; Heeger, A. J. *Proc. Natl. Acad. Sci. U.S.A.* **2010**, *107*, 10837.
(5) Ai, K.; Liu, Y.; Lu, L. *J. Am. Chem. Soc.* **2009**, *131*, 9496.
(6) Xie, X.; Xu, W.; Liu, X. *Acc. Chem. Res.* **2012**, *45*, 1511.
(7) Krishnan, S.; Mani, V.; Wasalathanthri, D.; Kumar, C. V.; Rusling, J. F. *Angew. Chem., Int. Ed.* **2011**, *50*, 1175.
(8) Aili, D.; Selegård, R.; Baltzer, L.; Enander, K.; Liedberg, B. *Small* **2009**, *5*, 2445.
(9) Clark, A. W.; Cooper, J. M. *Angew. Chem.* **2012**, *124*, 3622.
(10) Mirkin, C. A.; Letsinger, R. L.; Mucic, R. C.; Storhoff, J. J. *Nature* **1996**, *382*, 607.
(11) Elghanian, R.; Storhoff, J. J.; Mucic, R. C.; Letsinger, R. L.; Mirkin, C. A. *Science* **1997**, *277*, 1078.
(12) Lee, J. S.; Ulmann, P. A.; Han, M. S.; Mirkin, C. A. *Nano Lett.* **2008**, *8*, 529.
(13) Kim, S.; Eom, M. S.; Kim, S. K.; Seo, S. H.; Han, M. S. *Chem. Commun.* **2013**, *49*, 152.
(14) Kim, S.; Park, J. W.; Kim, D.; Lee, I. H.; Jon, S. *Angew. Chem.* **2009**, *121*, 4202.
(15) Liu, J.; Lu, Y. *J. Am. Chem. Soc.* **2004**, *126*, 12298.
(16) Xue, X.; Wang, F.; Liu, X. *J. Am. Chem. Soc.* **2008**, *130*, 3244.
(17) Jain, P. K.; El-Sayed, I. H.; El-Sayed, M. A. *Nano Today* **2007**, *2*, 18.
(18) Storhoff, J. J.; Lazarides, A. A.; Mucic, R. C.; Mirkin, C. A.; Letsinger, R. L.; Schatz, G. C. *J. Am. Chem. Soc.* **2000**, *122*, 4640.
(19) Thanh, N. T. K.; Rosenzweig, Z. *Anal. Chem.* **2002**, *74*, 1624.
(20) Storhoff, J. J.; Lucas, A. D.; Garimella, V.; Bao, Y. P.; Müller, U. R. *Nat. Biotechnol.* **2004**, *22*, 883.
(21) Lazarides, A. A.; Schatz, G. C. *J. Phys. Chem. B* **2000**, *104*, 460.
(22) Krpetić, Ž.; Guerrini, L.; Larmour, I. A.; Reglinski, J.; Faulds, K.; Graham, D. *Small* **2012**, *8*, 707.
(23) Nath, N.; Chilkoti, A. *Anal. Chem.* **2004**, *76*, 5370.
(24) Gonçalves, M. S. T. *Chem. Rev.* **2009**, *109*, 190.
(25) Wang, R. E.; Zhang, Y.; Cai, J.; Cai, W.; Gao, T. *Curr. Med. Chem.* **2011**, *18*, 4175.
(26) Opperwall, S. R.; Divakaran, A.; Porter, E. G.; Christians, J. A.; DenHartigh, A. J.; Benson, D. E. *ACS Nano* **2012**, *6*, 8078.
(27) Vallee-Belisle, A.; Ricci, F.; Plaxco, K. W. *J. Am. Chem. Soc.* **2012**, *134*, 2876.
(28) Taton, T. A.; Mirkin, C. A.; Letsinger, R. L. *Science* **2000**, *289*, 1757.
(29) Rosi, N. L.; Mirkin, C. A. *Chem. Rev.* **2005**, *105*, 1547.
(30) Chen, J. I.; Chen, Y.; Ginger, D. S. *J. Am. Chem. Soc.* **2010**, *132*, 9600.
(31) Chen, J. I. L.; Durkee, H.; Traxler, B.; Ginger, D. S. *Small* **2011**, *7*, 1993.
(32) Storhoff, J. J.; Elghanian, R.; Mucic, R. C.; Mirkin, C. A.; Letsinger, R. L. *J. Am. Chem. Soc.* **1998**, *120*, 1959.
(33) Lim, S.; Koo, O. K.; You, Y. S.; Lee, Y. E.; Kim, M. S.; Chang, P.-S.; Kang, D. H.; Yu, J.-H.; Choi, Y. J.; Gunasekaran, S. *Sci. Rep.* **2012**, *2*, 456.
(34) Fren, G. *Nature (London), Phys. Sci.* **1973**, *241*, 20.
(35) Liu, J.; Lu, Y. *Nat. Protoc.* **2006**, *1*, 246.
(36) Casado, A. G.; Rodriguez, L. C.; Hernandez, E. A.; Vilchez, J. L. *J. Chromatogr. A* **1996**, *726*, 133.
(37) Analytical Methods Committee.. *The Analyst* **1987**, *112*, 199.
(38) Sardar, R.; Tyler, B.; Shumaker-Parry, J. S. *J. Am. Chem. Soc.* **2007**, *129*, 5356.
(39) Xu, X.; Rosi, N. L.; Wang, Y.; Huo, F.; Mirkin, C. A. *J. Am. Chem. Soc.* **2006**, *128*, 9286.
(40) Li, W.; Camargo, P. H. C.; Lu, X.; Xia, Y. *Nano Lett.* **2008**, *9*, 485.
(41) Lattuada, M.; Hatton, T. A. *Nano Today* **2011**, *6*, 286.
(42) Jeffrey, N.; Hall, P. W.; Lyandres, O. *Nat. Mater.* **2008**, *7*, 442.
(43) Guo, L.; Chen, G.; Kim, D. H. *Anal. Chem.* **2010**, *82*, 5147.
(44) Guo, L.; Ferhan, A. R.; Lee, K.; Kim, D. H. *Anal. Chem.* **2011**, *83*, 2605.
(45) Guo, L.; Kim, D. H. *Biosens. Bioelectron.* **2012**, *31*, 567.
(46) Sonnichsen, C.; Reinhard, B. M.; Liphardt, J.; Alivisatos, A. P. *Nat. Biotechnol.* **2005**, *23*, 741.
(47) Reinhard, B. M.; Siu, M.; Agarwal, H.; Alivisatos, A. P.; Liphardt, J. *Nano Lett.* **2005**, *5*, 2246.
(48) Romero, I.; Aizpurua, J.; Bryant, G. W.; de Abajo, F. J. *Opt. Express* **2007**, *14*, 9988.
(49) Sheikholeslami, S.; Jun, Y.; Jain, P. K.; Alivisatos, A. P. *Nano Lett.* **2010**, *10*, 2655.
(50) Guo, L.; Ferhan, A. R.; Chen, H.; Li, C.; Chen, G.; Hong, S.; Kim, D. H. *Small* **2013**, *9*, 234.

(51) Feldkamp, U.; Niemeyer, C. M. *Angew. Chem., Int. Ed.* **2006**, *45*, 1856.
(52) Li, H.; Rothberg, L. *Proc. Natl. Acad. Sci. U.S.A.* **2004**, *101*, 14036.
(53) Han, M. S.; Lytton-Jean, A. K.; Oh, B. K.; Heo, J.; Mirkin, C. A. *Angew. Chem., Int. Ed.* **2006**, *45*, 1807.
(54) Xu, X.; Han, M. S.; Mirkin, C. A. *Angew. Chem.* **2007**, *119*, 3538.
(55) Zeng, Z.; Mizukami, S.; Kikuchi, K. *Anal. Chem.* **2012**, *84*, 9089.
(56) Balogh, D.; Zhang, Z.; Cecconello, A.; Vavra, J.; Severa, L.; Teply, F.; Willner, I. *Nano Lett.* **2012**, *12*, 5835.
(57) Choi, Y.; Ho, N. H.; Tung, C. H. *Angew. Chem., Int. Ed.* **2007**, *46*, 707.
(58) Jiang, Y.; Zhao, H.; Zhu, N.; Lin, Y.; Yu, P.; Mao, L. *Angew. Chem.* **2008**, *120*, 8729.
(59) Li, J.; Deng, T.; Chu, X.; Yang, R.; Jiang, J.; Shen, G.; Yu, R. *Anal. Chem.* **2010**, *82*, 2811.
(60) Reynolds, R. A.; Mirkin, C. A.; Letsinger, R. L. *J. Am. Chem. Soc.* **2000**, *122*, 3795.
(61) Xiao, N.; Yu, C. *Anal. Chem.* **2010**, *82*, 3659.
(62) Lin, Y.-W.; Huang, C.-C.; Chang, H.-T. *Analyst* **2011**, *136*, 863.
(63) Sung, Y. J.; Suk, H.-J.; Sung, H. Y.; Li, T.; Poo, H.; Kim, M.-G. *Biosens. Bioelectron.* **2013**, *43*, 432.
(64) Wang, Y.; Yang, F.; Yang, X. *ACS Appl. Mater. Interfaces* **2010**, *2*, 339.
(65) Lafleur, J. P.; Senkbeil, S.; Jensen, T. G.; Kutter, J. P. *Lab Chip* **2012**, *12*, 4651.
(66) Chen, Y.-Y.; Tseng, C.-W.; Chang, H.-Y.; Hung, Y.-L.; Huang, C.-C. *Biosens. Bioelectron.* **2011**, *26*, 3160.
(67) Ai, K.; Liu, Y.; Lu, L. *J. Am. Chem. Soc.* **2009**, *131*, 9496.
(68) Tseng, S.-C.; Yu, C.-C.; Wan, D.; Chen, H.-L.; Wang, L. A.; Wu, M.-C.; Su, W.-F.; Han, H.-C.; Chen, L.-C. *Anal. Chem.* **2012**, *84*, 5140.
(69) Lu, C. H.; Li, J.; Lin, M. H.; Wang, Y. W.; Yang, H. H.; Chen, X.; Chen, G. N. *Angew. Chem., Int. Ed.* **2010**, *49*, 8454.
(70) Xiao, X.; Song, C.; Zhang, C.; Su, X.; Zhao, M. *Chem. Commun.* **2012**, *48*, 1964.
(71) Zhao, Y.; Chen, F.; Wu, Y.; Dong, Y.; Fan, C. *Biosens. Bioelectron.* **2013**, *42*, 56.
(72) Sassolas, A.; Leca-Bouvier, B. D.; Blum, L. J. *Chem. Rev.* **2008**, *108*, 109.
(73) Liu, Y.; Shipton, M. K.; Ryan, J.; Kaufman, E. D.; Franzen, S.; Feldheim, D. L. *Anal. Chem.* **2007**, *79*, 2221.
(74) Mei, B. C.; Susumu, K.; Medintz, I. L.; Mattoussi, H. *Nat. Protoc.* **2009**, *4*, 412.
(75) Dixit, V.; Van den Bossche, J.; Sherman, D. M.; Thompson, D. H.; Andres, R. P. *Bioconjugate Chem.* **2006**, *17*, 603.
(76) Snyder, J. D.; Merson, M. H. *Bull. W. H. O.* **1982**, *60*, 605.
(77) Ashbolt, N. J. *Toxicology* **2004**, *198*, 229.
(78) Rosec, J.-P.; Causse, V.; Cruz, B.; Rauzier, J.; Carnat, L. *Int. J. Food Microbiol.* **2012**, *157*, 189.